APPLIED SCIENCES AND ENGINEERING

A dual-mode textile for human body radiative heating and cooling

Po-Chun Hsu,[1]* Chong Liu,[1] Alex Y. Song,[2] Ze Zhang,[3] Yucan Peng,[1] Jin Xie,[1] Kai Liu,[1] Chun-Lan Wu,[1] Peter B. Catrysse,[2] Lili Cai,[1] Shang Zhai,[3] Arun Majumdar,[3] Shanhui Fan,[2] Yi Cui[1,4]†

Maintaining human body temperature is one of the most basic needs for living, which often consumes a huge amount of energy to keep the ambient temperature constant. To expand the ambient temperature range while maintaining human thermal comfort, the concept of personal thermal management has been recently demonstrated in heating and cooling textiles separately through human body infrared radiation control. Realizing these two opposite functions within the same textile would represent an exciting scientific challenge and a significant technological advancement. We demonstrate a dual-mode textile that can perform both passive radiative heating and cooling using the same piece of textile without any energy input. The dual-mode textile is composed of a bilayer emitter embedded inside an infrared-transparent nanoporous polyethylene (nanoPE) layer. We demonstrate that the asymmetrical characteristics of both emissivity and nanoPE thickness can result in two different heat transfer coefficients and achieve heating when the low-emissivity layer is facing outside and cooling by wearing the textile inside out when the high-emissivity layer is facing outside. This can expand the thermal comfort zone by 6.5°C. Numerical fitting of the data further predicts 14.7°C of comfort zone expansion for dual-mode textiles with large emissivity contrast.

INTRODUCTION

Endothermy plays a pivotal role in maintaining proper function of humans. It is a subtle balance achieved by plenty of thermoregulation measures, such as metabolic rate, blood circulation, perspiration, pilo-erection (goose bumps), shivering, and so on (1). Failure to maintain core body temperature often results in severe medical emergencies. Today, although medical emergencies are much less common in daily life, thermal comfort is still heavily affecting our health, productivity, and economy (2). Indoor thermal comfort is generally achieved by air conditioning of the entire room or building, but it costs a considerable amount of energy (3, 4). In the United States, 12% of total energy consumption is for indoor temperature control (5–8). Without air conditioning, clothes become the only way to control human body temperature. However, common clothes have limited range of thermal insulation, which often fails to match up with the fluctuating weather. Large and sudden diurnal temperature variation can lead to respiratory infections and cardiac diseases (9, 10). These issues demand new effective ways to manage human body temperature. In particular, textile-based personal thermal management has great potential because it focuses the temperature control near the human body instead of the entire building (11–13).

Radiative thermal management has been shown to be an effective method for surpassing traditional ways of heating or cooling (14–17). By controlling emissivity, transmissivity, and reflectivity, different heat transfer controls can be achieved. For the human body at rest, infrared (IR) radiation (7 to 14 µm in wavelength) accounts for 40 to 60% of heat loss (18, 19). For personal heating, metallic nanowire coating onto regular textile has been demonstrated to reflect IR radiation back to the human body (12). Cooling textiles would require as much IR radiating

away from the human body, which has recently been demonstrated using nanoporous polyethylene (nanoPE) (11). NanoPE is transparent to mid-IR due to low absorption and little scattering, whereas it is opaque to human eyes due to strong scattering of visible light by the nanopores (50 to 1000 nm in diameter). Thus far, the opposite requirement of IR radiation control for heating and cooling has set the limit that one type of textile can only perform a single thermal function. It remains a grand challenge how to design a single textile to perform both heating and cooling functions. Although one can control the heat transfer from the sun, the wind, or from sweat evaporation, these extra heating/cooling sources are not always available in sufficient amount for effective controlling, especially for the indoor scenario. On the other hand, thermal radiation always exists and is the most universal heat transfer route for the human body. Practically, such a dual-mode textile would help the human body adapt to a wide range of ambient temperatures or physiological conditions. Traditionally, this can only be done by adding/removing the clothing or constantly adjusting the thermostat. However, extra clothing is not always available. Frequent changing of thermostat settings is inefficient and energy-wasting, and it often cannot satisfy all the residents at the same time. Here, we demonstrate a dual-mode textile for both heating and cooling by using a bilayer thermal emitter embedded inside the IR-transparent nanoPE. This dual-mode textile can easily switch modes between heating and cooling by flipping between inside and outside, which is considered passive and does not require electrical wiring or external energy input. The tunability of heat transfer coefficient can expand the thermal comfort zone and help the users adapt to the changing environment.

To understand the basic mechanism of a dual-mode textile, consider the radiation heat flux q_{rad} from human cloth toward the ambience

$$q_{rad} = \frac{\sigma(T_{tex}^4 - T_{amb}^4)}{\frac{1}{\varepsilon_{tex}} + \frac{1}{\varepsilon_{amb}} - 1} \approx \sigma\varepsilon_{tex}(T_{tex}^4 - T_{amb}^4) \tag{1}$$

where σ is the Stefan-Boltzmann constant, ε_{tex} is the textile surface emissivity, $\varepsilon_{amb} \approx 1$ is the ambience emissivity (20), T_{tex} is the textile surface temperature, and T_{amb} is the ambient temperature. For cooling

[1]Department of Materials Science and Engineering, Stanford University, Stanford, CA 94305, USA. [2]E. L. Ginzton Laboratory, Department of Electrical Engineering, Stanford University, Stanford, CA 94305, USA. [3]Department of Mechanical Engineering, Stanford University, Stanford, CA 94305, USA. [4]Stanford Institute for Materials and Energy Sciences, SLAC National Accelerator Laboratory, 2575 Sand Hill Road, Menlo Park, CA 94025, USA.
*Present address: Department of Mechanical Engineering, Stanford University, Stanford, CA 94305, USA.
†Corresponding author. Email: yicui@stanford.edu

or heating purposes, we would like to have either a high or a low q_{rad}, respectively. Therefore, to realize the dual-mode textile, both ε_{tex} and T_{tex} should be controllable. When ε_{tex} and T_{tex} are high, q_{rad} will increase, so human body heat dissipation becomes more efficient and the textile is in cooling mode. On the contrary, when ε_{tex} and T_{tex} are low, the textile is in heating mode. Traditional textiles are IR-opaque and have an emissivity of approximately 0.8 (21), which varies very little because of the similarity of the chemical composition of material choice. In most cases, both heat conduction and convection are symmetrical and invariable, so traditional textiles have only one fixed total heat transfer coefficient (see Fig. 1A and fig. S1A).

In our design, the bilayer thermal emitter, which has different emissivities on each side, is embedded inside the nanoPE textile, which also has asymmetric thicknesses on each side. Because the nanoPE is IR-transparent, the emitter inside it can freely radiate toward the ambience. The bilayer emitter can control the emissivity, and the nanoPE thickness controls the temperature of the emitter from being closer or farther from the hot side (human skin). In cooling mode (Fig. 1B), the high-emissivity layer (high ε_{tex}) is facing toward the environment, and the thickness of nanoPE between the emitter and the skin is small. This small thickness ensures efficient thermal conduction between the warm human skin and the emitter, which increases the emitter temperature (high T_{tex}). This combination of high emissivity (high ε_{tex}) facing outside and short emitter-to-skin distance (high T_{tex}) will result in high heat transfer coefficient, so the textile is in cooling mode. Ideally, if $\varepsilon_{tex} = \varepsilon_{skin} = 0.98$ (22) and the thermal resistance between the human skin and the emitter is zero ($T_{tex} = T_{skin}$), then the cooling effect will be as strong as wearing only the nanoPE cooling textile. When the textile is flipped, the low-emissivity side is facing out (low ε_{tex}), and the emitter-to-skin distance increases, resulting in lower thermal conductance (low T_{tex}); thus, the textile is in heating mode (Fig. 1C).

Note that the electromagnetic response of the structure in either heating or cooling mode is reciprocal. What varies between the heating and cooling mode is the difference temperature of the emitter. Neither is such a structure a photon-based thermal rectifier (23). In this case, the heating and cooling mode corresponds to different structure configuration between the high-temperature heat source (the human body) and the low-temperature heat sink (the ambient) (fig. S1). The dual modality is a synergistic result of radiation, conduction, and convection. When the mode switches, the radiation heat transfer components change, but the outside convection and the inside air gap conduction do not. The parallel and serial relationship among these heat transfer components will end up having two different effective heat transfer coefficients for two modes. Moreover, the IR transparency of nanoPE plays an indispensable role in achieving effective radiative cooling at the cooling mode while keeping the heating mode sufficiently warm. Although replacing nanoPE with an IR-opaque textile may still have asymmetrical heat transfer modes, its cooling power and dual modality will never be as good as the IR-transparent nanoPE. See the Supplementary Materials for the full analysis.

RESULTS AND DISCUSSION

To experimentally realize the dual-mode textile, the material choice and fabrication method of the bilayer emitter is important. Carbon has a large absorption coefficient in the range of mid-IR, approximately 28,000 to 87,000 cm^{-1} in the wavelength range of human body radiation (24–26), which makes it a great candidate for the high-emissivity layer. Figure 2A is the image of a 9-μm-thick carbon coating on the 12-μm-thick nanoPE by a doctor blade. The coating is rough and highly porous, rendering a dark and matte surface, which is advantageous for both high emissivity and air and vapor permeability (Fig. 2B) (27). On the other hand, the low-emissivity layer requires high reflectivity, so metal generally satisfies this criterion. We deposited 150 nm of copper onto nanoPE as the low-emissivity layer, which is smooth and shiny (Fig. 2C). Scanning electron microscopy (SEM) shows that the semiconformal copper coating is thin enough to leave the nanopores open, so the air and vapor permeability of the textile can be maintained (Fig. 2D). By sandwiching the two emitters face-to-face, the bilayer emitter structure is achieved, with nanoPE on both sides (Fig. 2E). An additional piece of nanoPE is added to the carbon side to create the thickness asymmetry. The final thickness of nanoPE is 24 μm at the carbon side and 12 μm at the copper side.

Besides morphological inspection, it is essential to measure the emissivity within the wavelength range of mid-IR to characterize the radiation heat transfer property. We use Fourier transform IR spectroscopy (FTIR) with the diffuse gold integrating sphere to probe the emissivities from both sides (Fig. 2F). The transmittance (τ) and the reflectivity (ρ) were measured to calculate the emissivity (ε) by $\varepsilon = 1 - \tau - \rho$. At the carbon side, the emissivity is approximately 0.8 to 1.0 between the wavelengths of 2 and 18 μm. The weighted average emissivity based on human
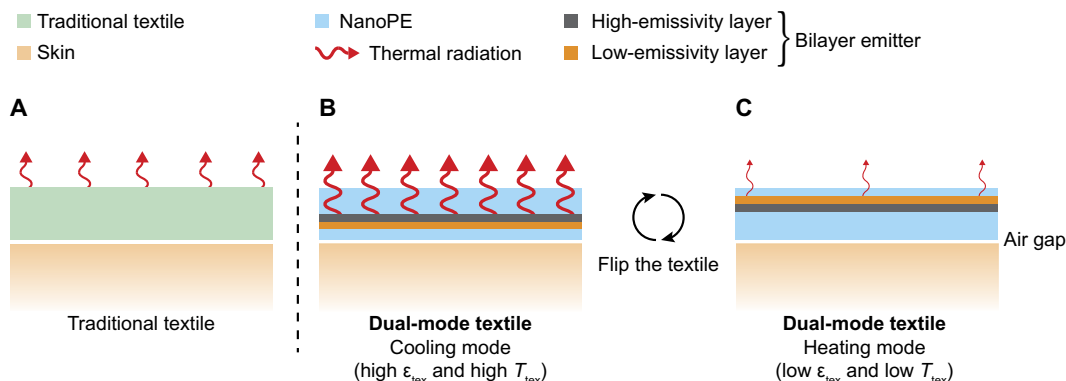
Fig. 1. Schematic of dual-mode textile. (A) Traditional textiles only have single emissivity, so the radiation heat transfer coefficient is fixed. **(B)** For a bilayer thermal emitter embedded in the IR-transparent nanoPE, when the high-emissivity layer faces outside and the nanoPE between the skin and the emitter is thin, the high emissivity and high emitter temperature results in large heat transfer coefficient, so the textile is in cooling mode. **(C)** The textile is flipped, and the low emissivity and low emitter temperature cause the heat transfer coefficient to decrease. The textile now works in heating mode.
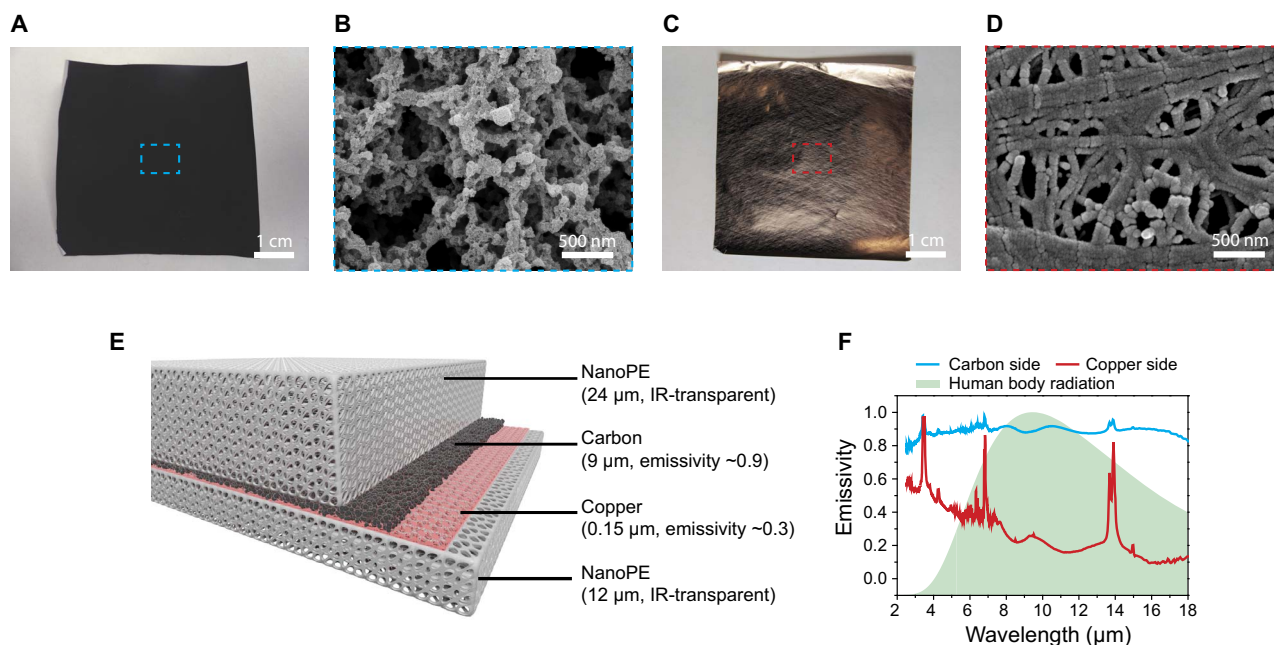
Fig. 2. Dual-mode textile morphology and emissivity characterization. (A) Image of a carbon-coated nanoPE, the high-emissivity layer. (B) SEM image of carbon coating reveals its rough and porous structure, which is advantageous for increasing the emissivity. (C) Image of a copper-coated nanoPE, the low-emissivity layer. (D) SEM image of copper coating shows that the surface is optically smooth for mid-IR. The nanopores remain open for air and vapor permeability. (E) Layered structure of the dual-mode textile. Note that the nanoPE on the side of carbon is thicker than the copper side. Note that all the materials are porous to allow air and vapor breathability. (F) Emissivities of carbon and copper coating, as measured by FTIR equipped with a diffuse gold integrating sphere.

body radiation at 33°C is 0.894. On the other hand, copper shows a much lower emissivity, with a weighted average value of 0.303. The strong absorption peaks at the wavelengths of 3.4, 3.5, 6.8, 7.3, 13.7, and 13.9 μm are attributed to polyethylene (28). These absorption peaks have little impact on the embedded emitters because they are sharp and far away from the central part of human body radiation.

The change of thermal insulation by mode switching and the influence of emissivity are demonstrated by the steady-state artificial skin temperature measurement with simulated metabolic heat generation and controllable ambient temperature in a clear acrylic chamber. The simulated metabolic heat generation is provided by an electric heater and is kept constant at 51 W/m² throughout the entire measurement, and the chamber temperature is kept constant at 22.0°C by a cooling/heating water recirculating system (fig. S3). The cooling and heating effect of the dual-mode textile is first demonstrated in Fig. 3A. Under the bare skin condition, the artificial skin temperature is 31.0°C. Placing a piece of traditional textile onto the artificial skin increases its temperature to 36.9°C. Here, we use a commercially available sweatshirt as the traditional textile sample. As for the dual-mode textile, when the carbon side (high emissivity) is facing outward, it works in cooling mode and causes the artificial skin temperature to decrease to 33.8°C. When the dual-mode textile is flipped inside out, with the copper (low-emissivity) facing outward, it works in heating mode and increases the artificial skin temperature to 40.3°C. This 6.5°C difference of artificial skin temperature is created by flipping the same piece of the dual-mode textile with exactly the same thickness and mass. Note that a few degrees Celsius change of artificial skin temperature due to cooling/heating can be translated to several tens of percents of energy savings for indoor temperature control (4). A sweating hotplate method was also used to test the dual modality under the influence of additional moisture evaporation (fig. S4). The result shows that even including the

evaporative heat loss, the cooling mode still has 10% higher total heat transfer coefficient than the heating mode. When considering evaporative heat loss, the traditional textile becomes a little warmer than the heating-mode textile. This means that water vapor does not propagate well in the traditional textile (a sweatshirt in this experiment) as compared to the dual-mode textile. We have thus demonstrated that flipping this textile results in markedly different thermal insulation properties. This dual modality could greatly enhance the adaptability of the human skin to the environment.

In the dual-mode textile design, the total heat transfer coefficient is closely related to the emissivities of bilayer emitters. By adjusting the coating thickness of the emitter, we can control its emissivity and achieve different extents of thermal property variation. We tested the artificial skin temperature of four dual-mode textiles with various emissivity combinations under both cooling and heating modes, so there are eight top-layer emissivities (ε_{top}) (Fig. 3B). The weighted average emissivities are computed on the basis of human body radiation. It is clear that the artificial skin temperature is inversely related to the top-layer emissivity, which determines the radiation heat transfer toward the ambience. On the other hand, the bottom-layer emissivity (ε_{bottom}) has little influence on the artificial skin temperature (fig. S6) because, between the skin and the bottom layer, the heat flux transporting through conduction is much larger than through radiation, so the bottom-layer emissivity has little impact on the overall heat transfer coefficient. The temperature difference created by the dual modality is plotted as the function of emissivity difference between the top and the bottom layer for each sample (Fig. 3C). We show that temperature tunability is predominantly controlled by the emissivity difference between the two emitting layers in the dual-mode textile. The samples with only copper and only carbon were also tested to confirm that the dual modality is not dependent on the absolute value of emissivities but on their difference (fig. S6).
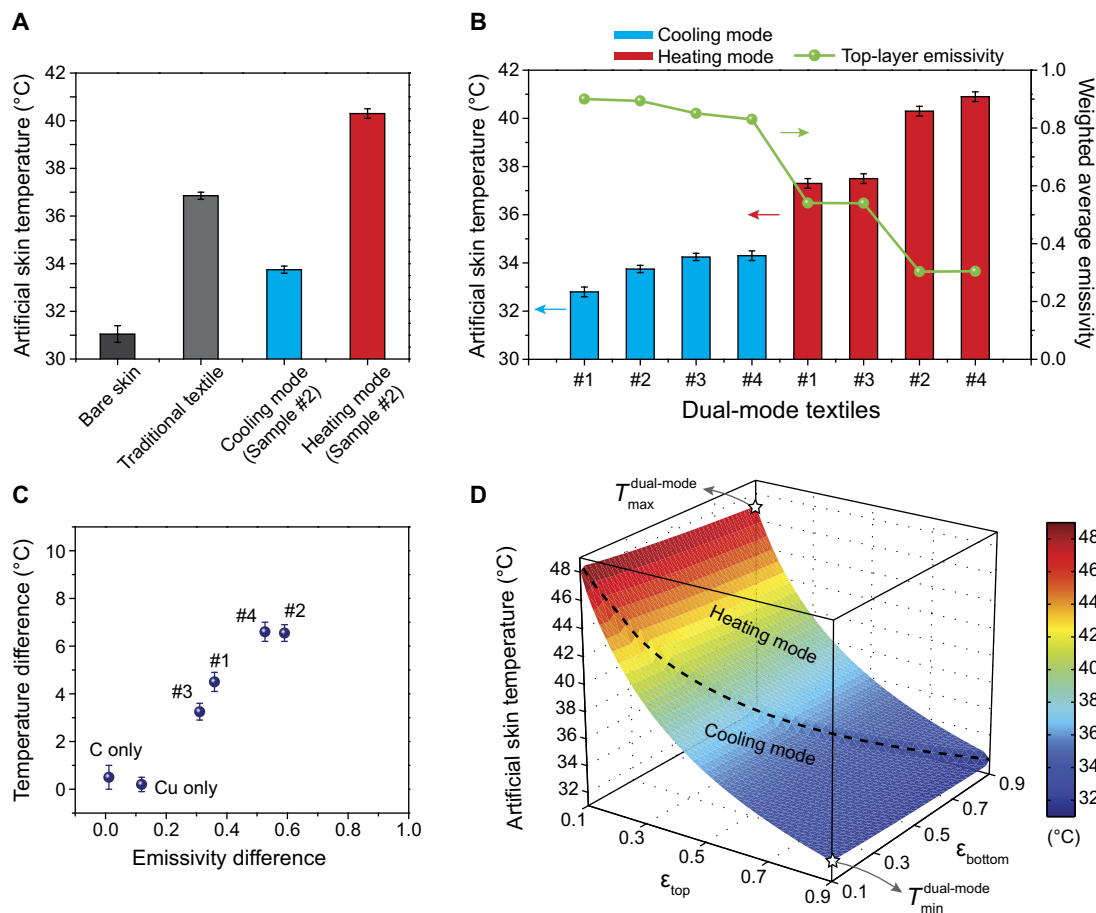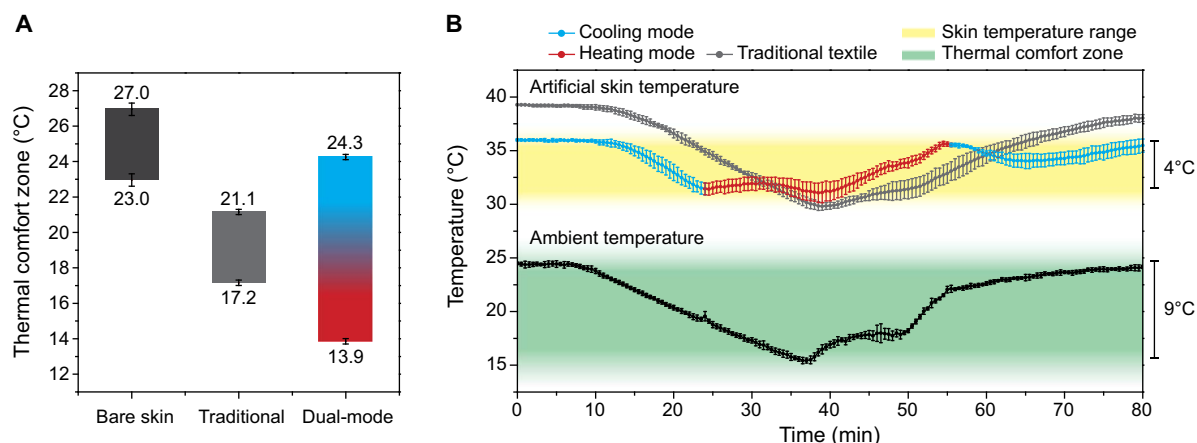
Fig. 3. Thermal measurement of the dual-mode textile. (**A**) Steady-state artificial skin temperature of various conditions: bare skin, traditional textile, cooling mode textile, and heating mode textile. The cooling and heating mode is the same piece of sample (#2) with different sides facing out, and the resulting artificial skin temperature is different. (**B**) Four dual-mode textiles with eight different top-layer emissivities result in different skin temperatures. The skin temperature is inversely related to the top-layer emissivity, which indicates the importance of radiation heat transfer toward the environment. (**C**) The temperature difference caused by mode switching is positively related to the emissivity difference between the two layers. Carbon-only and copper-only samples are also measured to verify that the dual modality does not depend on the absolute value of emissivity but on its difference. (**D**) Calculated artificial skin temperature as the function of top- and bottom-layer emissivities. The maximal temperature difference generated by the dual-mode textile occurs when $\Delta\varepsilon = 0.8$, which are marked with the star symbols.

To numerically predict the maximal temperature tunability in our current design, we fitted the thermal resistance of individual components and interfaces with thermal measurement and emissivity measurement data of the dual-mode textile samples. The equivalent thermal resistance circuit is shown in fig. S1. The fitted thermal resistances are then used to construct the heat transfer model and derive the relationship of skin temperature, ε_{top}, and ε_{bottom} (Fig. 3D). The dual-mode textile works in cooling mode when $\varepsilon_{top} > \varepsilon_{bottom}$ and in heating mode when $\varepsilon_{top} < \varepsilon_{bottom}$, as marked by the dotted line in Fig. 3D. We set the upper and lower limits of emissivity at 0.9 and 0.1, respectively, to better reflect the reality that the nanoPE has finite transmittance and the porous emitters may not achieve perfect reflectivity. The maximal temperature change occurs when $\Delta\varepsilon = 0.8$, that is, $(\varepsilon_{top}, \varepsilon_{bottom}) = (0.9, 0.1)$ for cooling and $(\varepsilon_{top}, \varepsilon_{bottom}) = (0.1, 0.9)$ for heating. Our calculation shows that this maximum dual-mode textile has $T_{max}^{dual\text{-}mode} = 47.1°C$ and $T_{min}^{dual\text{-}mode} = 32.4°C$, which correspond to $14.7°C$ of temperature variation. In practice, these emissivities could be realized by improving the coating method to maximize the absorption for the high-emissivity layer and the reflection for low-emissivity layer while maintaining the porosity and breathability. Further enhancement of

IR transmittance of nanoPE will also be helpful to take full advantage of the bilayer emitter design. This numerical modeling points out the largest possible tuning range of the dual-mode textile. To achieve thermal comfort, the heat transfer coefficient contrast and its average value should be optimally engineered to fit different scenarios.

The thermal comfort zone is defined as the range of ambient conditions that makes the residents feel comfortable. It is highly subjective and often requires polls and statistics to reach the consensus (*29*). As a proof of concept, we use artificial skin temperature as the indicator of thermal comfort and choose 32° to 36°C to be the comfortable range. In other words, the ambient temperature range that can result in the artificial skin temperature of 32° to 36°C is the thermal comfort zone. Depending on the thermal insulation property, different samples will have different thermal comfort zones, as measured by the steady-state thermal measurement device (Fig. 4A). Because the temperature change is relatively small and the heat transfer coefficients do not vary with temperature, the thermal comfort zone changes linearly with the artificial skin temperature and covers only 4°C for the case of bare skin and traditional textile. For the dual-mode textile, because it has two heat transfer coefficients, the thermal comfort zone ranges from

Fig. 4. Expansion of thermal comfort zone by the dual-mode textile. (**A**) Thermal comfort zone of bare skin, traditional textile, and dual-mode textile. The artificial skin temperature is between 32° and 36°C. (**B**) Real-time thermal measurements of dual-mode and traditional textiles under varying ambient temperatures. By using cooling mode at high ambient temperature and heating mode at low temperature, the artificial skin temperature stays within 32° to 36°C even if the ambient temperature changes between 16° and 25°C. In contrast, the traditional textile can only follow the trend of ambient temperature variation and result in thermal discomfort during the ambient temperature sweep. The error bars represent the SD of three measurements.

13.9° to 24.3°C, which is 10.4°C of coverage. Further real-time demonstration of the thermal comfort zone expansion by the dual-mode textile is shown in Fig. 4B, with traditional textile as a comparison. Note that the time-resolved thermal measurement is considerably affected by the thermal inertia, so the measured artificial skin temperatures are lagged behind the ambient temperature changes and are slightly different from the steady-state values in Fig. 4A. The error bars represent the SD of three independent measurements. As expected, the traditional textile can only follow the ambient temperature variation and provide thermal comfort in a small temperature range. As for the dual-mode textile, when the ambient temperature was so low that the artificial skin temperature almost fell below 32°C, the dual-mode textile was switched to heating mode and caused the artificial skin temperature to rise. Because the ambient temperature was still decreasing, the artificial skin temperature would eventually drop again until we started to increase the ambient temperature at 37 min. When the ambient temperature became too high, the textile was switched back to cooling mode. As a result, the dual-mode textile can maintain the artificial skin temperature within 32° to 36°C while encountering 9°C of dynamic ambient temperature fluctuation. This expansion of thermal comfort zone is carried out by simply flipping the sides of the textile and does not require any additional energy input, such as fossil fuels or electricity, which is particularly attractive for energy efficiency improvement and large-scale fabrication.

When designing the desirable emissivity, it is also important to maintain wearability as human clothing. In our previous report (*11*), we demonstrated several modification methods to improve the wearability of nanoPE, including polydopamine coating for hydrophilicity, microneedle punching for wind permeability, and embedding cotton mesh for mechanical strength. These modifications were shown to enhance the air permeability, water vapor transmissivity, mechanical strength, and wicking property of nanoPE (*11*). Similar wearability modification was performed on the dual-mode textile, as described in Materials and Methods. The thickness and the morphology of the bilayer emitter are specifically engineered, so the air and water vapor permeability of the dual-mode textile are similar to traditional textiles (fig. S7). Note that the higher water transmission rate of the dual-mode textile as compared to the sweatshirt is consistent with the sweating hot-plate measurement, as shown previously in fig. S4. Better engineering

of the hierarchical porous structure of nanoPE or fabrication of woven or knitted nanoPE as the IR-transparent layers should further increase its air permeability. Moreover, the microneedle-punched holes and the sewing threads only take a small percentage of the total area, and the hydrophilic polydopamine coating is extremely thin; thus, the overall emissivity and, therefore, the radiative property can be preserved (fig. S8). The dual-mode textile also shows decent durability against wash cycles because of the binder inside the carbon coating and the protection provided by the nanoPE/emitter/nanoPE sandwich structure (fig. S8). Printing, dyeing, or other deposition techniques that involve strong covalent or hydrogen bonds could be used to further improve the durability (*30–32*). The detergent/laundry machine wash cycle did cause artificial skin temperature to decrease for both heating and cooling modes. Given the similar emissivities after these wash cycles, we surmise that this decrease of thermal resistance is due to the residual detergent that reduces the contact resistance within the textile.

The core idea of the dual-mode textile for radiative cooling and heating is based on an asymmetrical thermal emitter embedded in the asymmetrical thickness of nanoPE. Flipping the same piece of the dual-mode textile would switch the radiative property and, therefore, the heat transfer coefficient. The wearers can then adapt to a wider range of ambient temperatures without the need to add or remove clothes. This wider adaptability means that the wearers do not need to sacrifice other functions of the clothes for thermal comfort, such as protection, social etiquette, utility, and so on. Because laws of thermodynamics guarantee the existence of thermal radiation that net-emits from warmer objects to the colder ambience, this radiative dual-mode textile has very wide applicability and does not require extra energy sources or triggers. This is particularly important for indoor scenarios where the sun, the wind, and human perspiration are either absent or very limited. The usage of IR-transparent nanoPE is also indispensable in the dual-mode textile. In fig. S9 and the Supplementary Materials, we explicitly calculate the skin temperatures for a dual-mode textile made of IR-transparent nanoPE and IR-opaque materials. Assuming that other thermal properties are the same, the dual-mode textile made of nanoPE can be very close to the bare skin limit, owing to its IR transparency. This also results in more significant dual modality than the IR-opaque counterpart.

Although the IR-transparent textile materials are fairly specific, the material choice for the bilayer emitter can be very broad. For the low-emissivity layer, aluminum and titanium are both highly reflective, cheap, stable, and nontoxic (fig. S10). For the high-emissivity layer, silicon dioxide and silicon nitride also have relatively high absorption coefficient at 9.5 μm, which are approximately 26,574 and 9362 cm^{-1}, respectively (33). This broad range of selection provides flexibility for satisfying more wearability requirements and for temperature range tunability. With this flexibility, the concept of radiative heating/cooling textiles would also be applicable to wearable electronics and benefit from each other. For example, wearable electronic devices would provide better control of the heat transfer modes or complement the radiative heating/cooling using thermoelectric or electrical heating, and the radiative heating/cooling textile could mitigate the negative impact of the electronic devices on personal thermal comfort.

MATERIALS AND METHODS
Materials
The nanoPE was from Entek International LLC (12 μm; Teklon). The traditional textile was a sweatshirt made of 60% cotton/40% polyester, brushed-back jersey (267 g/m^2 and 750 μm thick). The T-shirt textile, which was only used for wearability test, was a 100% cotton single jersey (130 g/m^2). Carbon slurry was made by dispersing one part of carbon black (Super C65, Imerys Graphite & Carbon) and one part of poly-acrylonitrile (molecular weight, 150,000; Sigma-Aldrich) in the proper amount of N,N′-dimethylformamide (>99.8%; Sigma-Aldrich). Silicon dioxide slurry was made by dispersing nine parts of 0.8-μm silicon dioxide powder prepared by the modified Stöber process (34) and one part of polyvinylidene difluoride (PVDF; melting point, 155° to 160°C; Alfa Aesar) in the proper amount of N-methyl-2-pyrrolidone (NMP; >99.0%; Sigma-Aldrich). Silicon nitride slurry was made by dispersing nine parts of silicon nitride powder (>99.9%; Sigma-Aldrich) and one part of PVDF in the proper amount of NMP. All slurry was rigorously stirred for at least 12 hours before use.

Bilayer emitter fabrication
The high-emissivity layer was made by doctor blade–coating the slurry that contains high-emissivity materials onto nanoPE. The doctor blade has changeable gauges for different coating thicknesses. The coated films were air-dried until the solvent completely evaporated before testing. The thicknesses were measured by a calibrated micrometer screw gauge. The carbon was 9 or 4 μm thick, the silicon dioxide was 199 μm thick, and the silicon nitride was 61 μm thick. The low-emissivity layers on nanoPE were all deposited by magnetron sputtering of various metals (AJA International), whose thicknesses were controlled by the sputtering power and time. The copper was 150 or 50 nm thick, the aluminum was 150 nm thick, and the titanium was 270 nm thick. The final samples for thermal and optical measurement were made by stacking the carbon- and copper-coated nanoPE together face-to-face, with an extra layer of pristine nanoPE next to the carbon-coated nanoPE, to achieve the structure shown in Fig. 2E. No adhesive was used.

Characterization
The SEM images were taken by FEI XL30 Sirion (5 kV). The IR properties were measured by an FTIR spectrometer (model 6700, Thermo Fisher Scientific) accompanied with a diffuse gold integrating sphere (PIKE Technologies). Unless specified, the incident angle to the sam-

ple is 12°. The FTIR was used to measure reflectivity (ρ) and transmissivity (τ), and the emissivity (ε) was calculated on the basis of ε = 1 − ρ − τ.

Thermal measurement
We used the steady-state, constant heat flux setup to measure the total heat transfer coefficient of the textile samples (fig. S3). The artificial skin was a silicone rubber electric heater (9 cm × 8 cm) with a k-type thermocouple (SA1-K, OMEGA Engineering) attached on the center of the top surface, denoted as T_{skin}. A guard heater (9 cm × 8 cm) was placed below the artificial skin with a k-type thermocouple (SA1-K, OMEGA Engineering) attached on the center of the bottom surface, denoted as T_{guard}, which is always kept the same as T_{skin}, so the interface between the main heater and the guard heater can be regarded as an insulating boundary. Therefore, the heat generation of the main heater can be treated as a one-dimensional upward heat flux, denoted as q. All the electronic equipment listed above was purchased from OMEGA Engineering. The artificial skin and the tested sample were enclosed in an IR-opaque, visibly transparent acrylic chamber (TAP Plastics) with circulating water to control the chamber air temperature, denoted as T_{amb} (Cole-Parmer), which was measured by a k-type thermocouple located 15 cm above the center of the sample. For all thermal measurements except the real-time comfort zone measurement (Fig. 4B), T_{amb} = 22°C and q = 51 W/m^2. When textiles with different heat transfer coefficients are placed onto the artificial skin or when T_{amb} changes, T_{skin} will change accordingly. The textile samples were all 5 cm × 5 cm in size. A 220-μm-thick duct tape was used to cover the area without sample and prevent heat loss from the edges.

Sweating hotplate thermal measurement
The sweating hotplate was based on the basic components of normal thermal measurement but with an additional metal foam water container for simulating perspiration (fig. S4). The experimental method was based on ASTM F1868 with modification. The metal foam was thermally insulated by fiberglass tapes, and a waterproof and vapor-permeable film was covered on the top of the metal foam to protect the textile sample from contact with water. We used an untreated nanoPE film as the waterproof vapor-permeable film, although other hydrophobic porous films, such as Teflon, are also suitable for this purpose. To achieve the constant vapor pressure between the artificial skin and the textile constant, we adjusted the heat flux to maintain the same artificial skin temperature (35 ± 0.1°C) for all measurements. The ambient temperature was controlled by the water recirculation system at 19 ± 0.1°C, and the chamber was large enough to keep the relative humidity within 30 ± 5%. Both the ambient temperature and the relative humidity were measured using a digital hygrometer (Thermo Fisher Scientific). The total heat transfer coefficient was finally calculated by the applied heat flux, the artificial skin temperature, and the ambient temperature.

Wearable nanoPE modification
The wearability modification for the dual-mode textile was based on the study of Pérez-Lombard et al. (7). First, the nanoPE was perforated by microneedle arrays (AdminPatch 300, nanoBioSciences) or 30-gauge needles (BD PrecisionGlide). Second, it was coated with polydopamine by pH-induced polymerization for 24 hours. The coating solution was composed of dopamine hydrochloride (2 g/liter; Sigma-Aldrich), tris-HCl (10 mM; pH 8.5; Teknova), and 50 weight % methanol/water solution. The processed nanoPE was then coated with

the high-/low-emissivity layer and sewn together by a sewing machine within the same sequence as Fig. 2E. The sewing threads are made of polyester and have a grid-like pattern with a mesh size of 1 cm × 1 cm (2).

Water vapor transmission rate test

The testing procedure was based on ASTM E96 with modification. Media bottles (100 ml) (Thermo Fisher Scientific) were filled with 20 ml of distilled water. The bottles were sealed by the textile samples using open-top caps and silicone gaskets (Corning). The exposed area of textile was 35 mm in diameter. The sealed bottles were then placed into an environmental chamber where the temperature was held at 35°C and the relative humidity was 30 ± 10%. The mass of the bottles and the samples was measured periodically, and the reduced mass should come from the evaporated water. The reduced mass was then divided by the area to derive the water vapor transmission.

Air permeability test

The testing procedure was based on ASTM D737, with modification. Textile samples were sealed between two pipes using flange adapters, a centering O-ring, and a clamp. The exposed area of the textile was 17.3 mm in diameter. One pipe was connected to a T-connector at the short/straight leg and then connected to the compressed air source. The other pipe was also connected to a T-connector at the short/straight leg and then connected to open air. In other words, the air flows straight through the pipe and the textile. A differential pressure gauge (UEi Test Instruments) was connected to both long/branch legs to measure the pressure drops across the textile sample at different air flow rates.

Wicking test

The testing procedure was based on AATCC (American Association of Textile Chemists and Colorists) TM 197, with modification. The textile samples were cut into 2-cm-wide strips and dipped into distilled water. The water started to climb up the sample due to capillary force. The climbing duration was 10 s.

Mechanical test

The strip tensile strength test was measured by Instron 5565. The sample size was 25 mm wide and 5 cm long, and the gauge distance was 4 cm long. The displacement rate was 10 mm/min.

SUPPLEMENTARY MATERIALS

Supplementary material for this article is available at http://advances.sciencemag.org/cgi/content/full/3/11/e1700895/DC1

Supplementary Text

fig. S1. Thermal circuit model of textiles.
fig. S2. Direct copper deposition on carbon/nanoPE.
fig. S3. Schematic of thermal measurement apparatus.
fig. S4. Sweating hotplate thermal measurement.
fig. S5. Emissivities of samples #1 to #4 used in the experiments.
fig. S6. Complete thermal measurement and weighted average emissivity of various samples.
fig. S7. Wearability tests of dual-mode textile, T-shirt, and sweatshirt.
fig. S8. Performance durability of dual-mode textile against wash cycles.
fig. S9. Comparison between IR-transparent and IR-opaque dual-mode textiles.
fig. S10. Emissivities of alternative materials for bilayer emitters.
fig. S11. Calculated comfortable ambient temperature as the function of top- and bottom-layer emissivities at T_{skin} = 34°C.
fig. S12. Guarded hotplate setup for thermal conductivity measurement.
fig. S13. Emissivity spectrum of the traditional textile.
fig. S14. Weighted average emissivities of heating mode, cooling mode, and traditional textiles as a function of temperature.
fig. S15. Overlay of thermal measurement data on the numerical fitting result.

fig. S16. Measurement of specular, diffuse, and angle-dependent emissivities.
table S1. Thickness of dual-mode textiles.
table S2. Numerically fitted values of heat transfer components.
table S3. Thermal properties of the dual-mode and the traditional textiles measured by guarded hotplate method.
References (35, 36)

REFERENCES AND NOTES

1. T. S. Kemp, The origin of mammalian endothermy: A paradigm for the evolution of complex biological structure. *Zool. J. Linn. Soc.* **147**, 473–488 (2006).
2. T. A. Carleton, S. M. Hsiang, Social and economic impacts of climate. *Science* **353**, aad9837 (2016).
3. S. Chu, A. Majumdar, Opportunities and challenges for a sustainable energy future. *Nature* **488**, 294–303 (2012).
4. T. Hoyt, H. L. Kwang, H. Zhang, E. Arens, T. Webster, Energy savings from extended air temperature setpoints and reductions in room air mixing, paper presented at the International Conference on Environmental Ergonomics, Boston, MA, 2 to 7 August 2009.
5. U.S. Energy Information Administration, *Annual Energy Outlook 2016 with Projections to 2040* (U.S. Energy Information Administration, Office of Energy Analysis, 2016).
6. J. D. Kelso, *2011 Buildings Energy Data Book* (U.S. Department of Energy, 2012).
7. L. Pérez-Lombard, J. Ortiz, C. Pout, A review on buildings energy consumption information. *Energ. Buildings* **40**, 394–398 (2008).
8. T. Bryant, S. Thomas, B. Dean, L. Lyons, D. Morgado, K.-H.Je, D. Subkhankulova, E. Dennehy, Y. Liu, D. Houssin, *Medium Term Energy Efficiency Market Report 2015* (International Energy Agency, 2015).
9. J. C. Heunis, J. Olivier, D. E. Bourne, Short-term relationships between winter temperatures and cardiac disease mortality in Cape Town. *S. Afr. Med. J.* **85**, 1016–1019 (1995).
10. F. T. Chew, S. Doraisingham, A. E. Ling, G. Kumarasinghe, B. W. Lee, Seasonal trends of viral respiratory tract infections in the tropics. *Epidemiol. Infect.* **121**, 121–128 (1998).
11. P.-C. Hsu, A. Y. Song, P. B. Catrysse, C. Liu, Y. Peng, J. Xie, S. Fan, Y. Cui, Radiative human body cooling by nanoporous polyethylene textile. *Science* **353**, 1019–1023 (2016).
12. P.-C. Hsu, X. Liu, C. Liu, X. Xie, H. R. Lee, A. J. Welch, T. Zhao, Y. Cui, Personal thermal management by metallic nanowire-coated textile. *Nano Lett.* **15**, 365–371 (2015).
13. J. K. Tong, X. Huang, S. V. Boriskina, J. Loomis, Y. Xu, G. Chen, Infrared-transparent visible-opaque fabrics for wearable personal thermal management. *ACS Photonics* **2**, 769–778 (2015).
14. N. N. Shi, C.-C. Tsai, F. Camino, G. D. Bernard, N. Yu, R. Wehner, Keeping cool: Enhanced optical reflection and radiative heat dissipation in Saharan silver ants. *Science* **349**, 298–301 (2015).
15. A. P. Raman, M. A. Anoma, L. Zhu, E. Rephaeli, S. Fan, Passive radiative cooling below ambient air temperature under direct sunlight. *Nature* **515**, 540–544 (2014).
16. L. Zhu, A. P. Raman, S. Fan, Radiative cooling of solar absorbers using a visibly transparent photonic crystal thermal blackbody. *Proc. Natl. Acad. Sci.* **112**, 12282–12287 (2015).
17. O. Ilic, P. Bermel, G. Chen, J. D. Joannopoulos, I. Celanovic, M. Soljačić, Tailoring high-temperature radiation and the resurrection of the incandescent source. *Nat. Nanotechnol.* **11**, 320–324 (2016).
18. J. D. Hardy, E. F. DuBois, Regulation of heat loss from the human body. *Proc. Natl. Acad. Sci. U.S.A.* **23**, 624–631 (1937).
19. C.-E. A. Winslow, A. P. Gagge, L. P. Herrington, The influence of air movement upon heat losses from the clothed human body. *Am. J. Physiol.* **127**, 505–518 (1939).
20. J. H. Lienhard, J. H. Lienhard, *A Heat Transfer Textbook* (Phlogiston Press, ed. 3, 2016).
21. M. Mason, I. Coleman, "Study of the surface emissivity of textile fabrics and materials in the 1 to 15 μm range" (Technical Report 67-86-CM, Clothing and Organic Materials Division, U.S. Army Natick Laboratories, 1967).
22. J. Steketee, Spectral emissivity of skin and pericardium. *Phys. Med. Biol.* **18**, 686–694 (1973).
23. C. R. Otey, W. T. Lau, S. Fan, Thermal rectification through vacuum. *Phys. Rev. Lett.* **104**, 154301 (2010).
24. A. Borghesi, G. Guizzetti, *Handbook of Optical Constants of Solids* (Academic Press, 1997), vol. 2.
25. H.-J. Hagemann, W. Gudat, C. Kunz, Optical constants from the far infrared to the x-ray region: Mg, Al, Cu, Ag, Au, Bi, C, and Al₂O₃. *J. Opt. Soc. Am.* **65**, 742–744 (1975).
26. W. H. Dalzell, A. F. Sarofim, Optical constants of soot and their application to heat-flux calculations. *J. Heat Transfer* **91**, 100–104 (1969).
27. C.-D. Wen, I. Mudawar, Modeling the effects of surface roughness on the emissivity of aluminum alloys. *Int. J. Heat Mass Transf.* **49**, 4279–4289 (2006).

28. J. V. Gulmine, P. R. Janissek, H. M. Heise, L. Akcelrud, Polyethylene characterization by FTIR. *Polym. Test.* **21**, 557–563 (2002).

29. B. W. Olesen, Thermal comfort. *Tech. Rev.* **2**, 3–41 (1982).

30. Z. Zhao, C. Yan, Z. Liu, X. Fu, L.-M. Peng, Y. Hu, Z. Zheng, Machine-washable textile triboelectric nanogenerators for effective human respiratory monitoring through loom weaving of metallic yarns. *Adv. Mater.* **28**, 10267–10274 (2016).

31. T. L. Vigo, *Textile Processing and Properties: Preparation, Dyeing, Finishing and Performance*, vol. 11 of *Textile Science and Technology* (Elsevier Science, 1994).

32. M. M. El-Molla, R. Schneider, Development of ecofriendly binders for pigment printing of all types of textile fabrics. *Dyes Pigm.* **71**, 130–137 (2006).

33. J. Kischkat, S. Peters, B. Gruska, M. Semtsiv, M. Chashnikova, M. Klinkmüller, O. Fedosenko, S. Machulik, A. Aleksandrova, G. Monastyrskyi, Y. Flores, W. T. Masselink, Mid-infrared optical properties of thin films of aluminum oxide, titanium dioxide, silicon dioxide, aluminum nitride, and silicon nitride. *Appl. Optics* **51**, 6789–6798 (2012).

34. W. Stöber, A. Fink, E. Bohn, Controlled growth of monodisperse silica spheres in the micron size range. *J. Colloid Interface Sci.* **26**, 62–69 (1968).

35. H. Maleki, S. A. Hallaj, J. R. Selman, R. B. Dinwiddie, H. Wang, Thermal properties of lithium-ion battery and components. *J. Electrochem. Soc.* **146**, 947–954 (1999).

36. S. C. Chen, C. C. Wan, Y. Y. Wang, Thermal analysis of lithium-ion batteries. *J. Power Sources* **140**, 111–124 (2005).

Science Advances

A dual-mode textile for human body radiative heating and cooling

Po-Chun Hsu, Chong Liu, Alex Y. Song, Ze Zhang, Yucan Peng, Jin Xie, Kai Liu, Chun-Lan Wu, Peter B. Catrysse, Lili Cai, Shang Zhai, Arun Majumdar, Shanhui Fan and Yi Cui

ARTICLE TOOLS	http://advances.sciencemag.org/content/3/11/e1700895
SUPPLEMENTARY MATERIALS	http://advances.sciencemag.org/content/suppl/2017/11/06/3.11.e1700895.DC1
REFERENCES	This article cites 28 articles, 6 of which you can access for free http://advances.sciencemag.org/content/3/11/e1700895#BIBL
PERMISSIONS	http://www.sciencemag.org/help/reprints-and-permissions

Use of this article is subject to the Terms of Service